Journal of Applied Electrochemistry **32**: 1331–1336, 2002.

Hydrogen incorporation in Ni–P films prepared by electroless deposition

M. SAAOUDI[1,2], E. CHASSAING[2,*], M. CHERKAOUI[1] and M. EBNTOUHAMI[1]
[1]*Laboratory of Electrochemistry and Surface Treatments, Faculty of Sciences, University Ibn Tofail, Kenitra, Morocco;*
[2]*Centre d'Etudes de Chimie Métallurgique, CNRS, 94407 Vitry-sur-Seine Cedex, France*
*(*author for correspondence, e-mail: elisabeth.chassaing@glvt-cnrs.fr)*

Received 11 March 2002; accepted in revised form 18 August 2002

Key words: electroless deposition kinetics, hydrogen incorporation, Ni–P films, quartz crystal microbalance

Abstract

Electroless NiP films, with 12 to 16 wt % P, were deposited from a moderately acid solution. Thermogravimetric analysis indicates the presence of occluded hydrogen in the layers, which desorbs upon heating. The amount of incorporated hydrogen decreases when the pH of the solution or the nickel sulfate concentration is increased; by contrast it increases with hypophosphite concentration. Cyclic voltammetry, using an electrochemical quartz crystal microbalance, confirms the existence of parasitic reactions, namely the reduction of protons of the solvent during the cathodic process and oxidation of hydrogen during the dissolution of the layers. This behaviour is in qualitative agreement with the proposed reaction scheme.

1. Introduction

Electroless nickel is largely employed due to the specific properties of the layers, that is, amorphous structure with high thermal stability, wear resistance, corrosion protection, and non-magnetic properties [1–4]. These coatings are used in the automobile and food industries [5]. More recently they have been used in the electronic microcircuits and packaging [6].

In previous work we have developed an ammoniacal solution. High quality Ni–P and Ni–Cu–P films have been prepared showing good corrosion properties [7, 8]. The kinetics of the deposition process were analysed [9]. These alkaline electrolytes are useful for deposition on non-conducting materials, such as glass or plastic substrates [3]. In the present work we investigate moderately acid solutions, which are commonly used in most industrial processes. To gain information on the properties and the deposition kinetics of the NiP films, two kinds of experiments were carried out. (i) The amount of incorporated hydrogen was measured using thermodesorption on NiP electrolessly deposited films. Indeed it is known that the parasitic hydrogen evolution and trapping of hydrogen may induce corrosion fatigue of the substrate [10] and brittleness of the Ni–P layers [11]. (ii) Cyclic voltammetry using an electrochemical quartz crystal microbalance allows investigation of the electrochemical reactions involved in the electroless process. We focus on the deposition and dissolution efficiencies and relate these characteristics to the presence of occluded hydrogen, which is codeposited. A reaction scheme is discussed in the light of the results.

2. Experimental procedure

The composition of the basic solution, denoted electrolyte 1b (Table1), was derived from a previous investigation [8]. It contained nickel sulfate (0.1 M dm^{-3} $NiSO_4$, $6H_2O$), sodium hypophosphite (0.28 M dm^{-3} NaH_2PO_2, H_2O) and sodium citrate (0.2 M dm^{-3} $Na_3C_6H_5O_7$, 2 H_2O). The temperature was held at 87 ± 2 °C. The solution was deaerated by nitrogen bubbling. The pH was varied between 4 and 6 by addition of acetic acid, which acts as a buffering agent in this pH range (pK_a 4.8). The influence of hypophosphite and nickel sulfate concentrations was also investigated (Table 1).

The reference electrode was a saturated calomel electrode (SCE), against which all potentials were measured. The counter electrode was a platinum wire. The substrate was a copper plate (2 cm^2), which was degreased and etched in dilute sulfuric acid prior to the experiment. Since copper does not catalyse the electroless process, a nickel strike was deposited from a Watts solution at −1600 mV, before the immersion in the electroless bath.

The phosphorus content of the alloys was determined by ICP analysis after dissolution of the layers or by EDX in the scanning electron microscope. X-ray diffraction

Table 1. Composition of the electrolytes (M dm^{-3})

Electrolyte	NaH_2PO_2, H_2O	$NiSO_4$, $6H_2O$	$Na_3C_6H_5O_7$, $2H_2O$	pH
1a	0.28	0.10	0.2	**4**
1b (basic)	0.28	0.10	0.2	5
1c	0.28	0.10	0.2	**6**
2a	**0.10**	0.10	0.2	5
2c	**0.40**	0.10	0.2	5
3a	0.28	**0.05**	0.2	5
3c	0.28	**0.15**	0.2	5

was performed using a Philips diffractometer with a cobalt anticathode ($\lambda_{K\alpha} = 0.178\ 89$ nm).

To characterize the thermal stability of the Ni–P alloys, differential scanning microcalorimetry was carried out, using a Perkin–Elmer calorimeter and a scan rate of 20 °C min^{-1}, up to 500 °C. The heat flow was calibrated using zinc fusion. Thermogravimetry was performed, under an argon flow, up to 400 °C, with a scan rate of 10 °C min^{-1}. The mass loss was calibrated using baryum chloride ($BaCl_2$, $2\ H_2O$). For these experiments the layers were deposited on thin copper foils, peeled off and weighed just before the thermogravimetric analysis.

Cyclic voltammetry was carried out using an electrochemical quartz crystal microbalance (EQCM) coated with a gold film, and a scan rate of 10 mV s^{-1}. The experiments were monitored by means of a microcomputer and homemade softwares [8]. For these experiments, the bath temperature was held at 40 °C. The microbalance was calibrated using a solution containing 0.5 M $CuSO_4$, 0.5 M H_2SO_4 and 1.1 M C_2H_5OH, for which the faradaic efficiency is close to unity [12]. The Sauerbrey coefficient was calculated equal to 56.7 ± 0.3 Hz μg^{-1} cm^2.

3. Results

3.1. *General considerations*

The plating rate, obtained with the basic solution (electrolyte 1b) at pH 5 and 87 °C, is 4.5 μm h^{-1} [13]. The rate increases with the pH of the solution, from 1 μm h^{-1} at pH 4 to 6 μm h^{-1} at pH 6. As expected, the plating rate also increases with both hypophosphite and nickel sulfate concentration (Table 2).

The phosphorus content decreases slightly from 14.7 wt % to 12.5 wt %, when the pH is increased from 4 to 6; from 15.5% to 10.0% when the nickel sulfate concentration is increased from 0.050 M to 0.15 M; and from 14.5% to 13.5% when the hypophosphite concentration is diminished from 0.4 M to 0.1 M.

As expected for Ni–P alloys with phosphorus content greater than 12 at % [14], these alloys are amorphous: the X-ray diffraction patterns show only a broad halo at 2θ around 50° with a half-height width of 10°.

Table 2. Plating rate (v) measured at the deposition potential (μm h^{-1}), phosphorus content τ_P (wt %) and hydrogen uptake in the films $\Delta m_{H(inc.)}/\Delta m_{film}$ (g g^{-1})

Electrolyte	v	τ_P	$\Delta m_{H(inc.)}/\Delta m_{film}$
1a	1.0	14.7	18.5×10^{-3}
1b (basic)	4.6	14.3	10.0×10^{-3}
1c	6.0	12.5	4.8×10^{-3}
2a	0.5	13.5	0.5×10^{-3}
2c	6.5	14.5	6.2×10^{-3}
3a	1.5	15.5	16.0×10^{-3}
3c	5.0	10.0	8.4×10^{-3}

3.2. *Thermal stability*

In agreement with other investigations [14, 15], the DSC curves obtained for nickel alloys with P contents greater than 20 at %, exhibit two well-defined exothermic features (Figure 1). This indicates a two-step crystallization at temperatures of 317 ± 1 °C and 394 ± 1 °C, respectively. The exact nature of the phases formed is still a matter of discussion [14–16]. The first peak is likely to the crystallization into the metastable phase Ni_5P_2 (supersaturated with nickel). The second is attributable to recrystallization of this metastable phase into Ni_3P and Ni precipitation, and possibly to grain growth [14, 15]. The heats evolved during these processes are respectively 67 J g^{-1} and 22 J g^{-1}, which compare well with the values cited for electrodeposited Ni–P alloys by Bakonyi et al. [14]. In addition to these well-defined peaks, a broad shoulder, corresponding to an exothermic process, is observed at lower temperatures. This is often observed for amorphous materials, and is related to the structural relaxation of the sample.

The XRD investigation confirms the amorphous structure of the as-deposited films. The half-height width decreases only slightly on annealing at 200 °C. After annealing at 380°, the alloys show the pattern of Ni_5P_2.

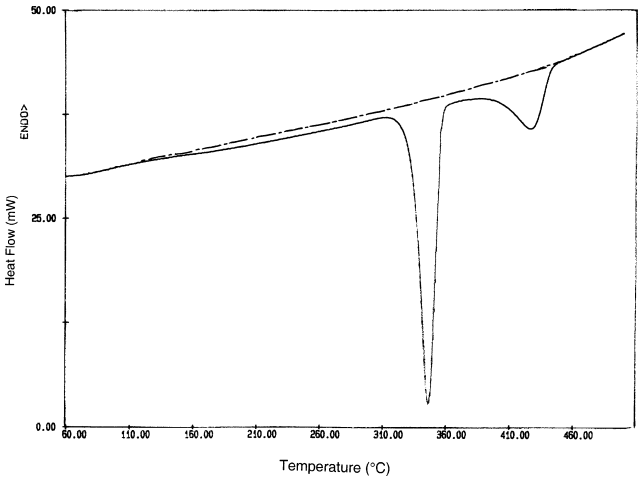

Fig. 1. DSC curve of a Ni–P films (13 wt % P) deposited from the basic solution at pH 5 and 87 °C. Scan rate 20 °C min^{-1}.

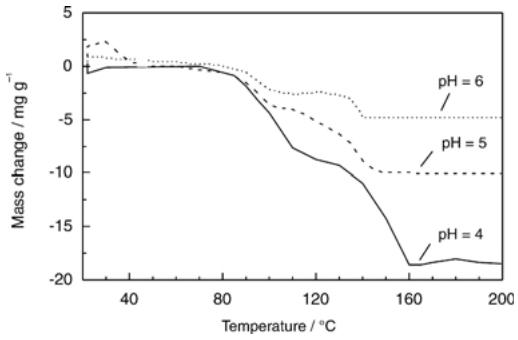

Fig. 2. Influence of the pH value of the plating solution on the thermodesorption behaviour of Ni–P films separated from the substrate. Scan rate 10 °C min^{-1}. Curves: (1) pH 4 (solid line), (2) pH 5 (dashed line) and (3) pH 6 (dotted line).

After heat treatment at 600°, the alloys exhibit the patterns of Ni_5P_2 and Ni_3P, in agreement with [14, 15].

3.3. *Thermogravimetric investigation*

It is known that electroless process is accompanied by hydrogen evolution which may be incorporated into the deposit [3]. To characterize the amount of occluded gas, a thermogravimetric investigation was undertaken. The electroless NiP films were heated to 400 °C under an argon flow and the mass changes were recorded.

Figure 2 shows the response of NiP films deposited at different pH. After a small increase at 30–40 °C, probably due to slight oxidation of the films, the mass decreases in two steps: the first step for a temperature around 85 °C and the second step around 125 °C. Both mass changes are of the same order. The mass decrease is larger, the lower the pH. Figures 3 and 4 show the response for films deposited from the other solutions. The weight loss decreases as the nickel concentration in the bath increases (Figure 3). It does not change markedly when the hypophosphite concentration is increased from 0.1 to 0.28 M, but it increases strongly when the concentration is further increased to 0.4 M (Figure 4). The results are summarized in Table 2.

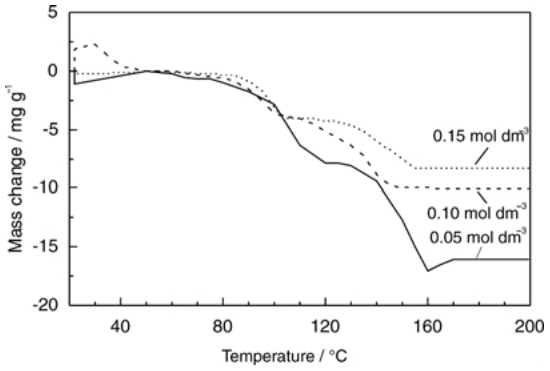

Fig. 3. Influence of the nickel sulphate concentration of the plating solution on the thermodesorption behaviour of Ni–P films separated from the substrate. Scan rate 10 °C min^{-1}. Curves: (1) 0.05 M $NiSO_4$ (solid line), (2) 0.10 M $NiSO_4$ (dashed line) and (3) 0.15 M $NiSO_4$ (dotted line).

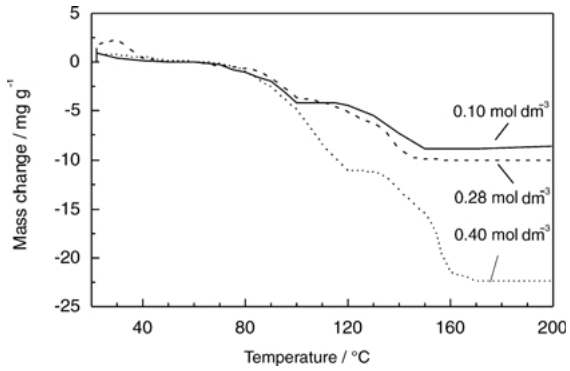

Fig. 4. Influence of the hypophosphite concentration of the plating solution on the thermodesorption behaviour of Ni–P films separated from the substrate. Scan rate 10 °C min^{-1}. Curves (1) 0.10 M NaH_2PO_2 (solid line), (2) 0.28 M NaH_2PO_2 (dashed line) and (3) 0.40 M NaH_2PO_2 (dotted line).

3.4. *Cyclic voltammetric investigation*

A voltammetric investigation was carried out using an electrochemical quartz crystal microbalance (EQCM), to identify the different reduction and oxidation steps. Indeed, although the net current at the deposition potential is equal to zero, the electroless process is essentially an electrochemical process. This results from anodic and cathodic reactions which, however, are not independent [3]. As for corrosion processes, to gain information on the kinetics it is necessary to investigate both anodic and cathodic reactions.

The EQCM allows calculation of the deposited or dissolved mass from frequency changes using Sauerbrey's equation. By comparing these mass changes with those calculated from Faraday's law, the efficiencies of the deposition or dissolution processes can be determined.

Figure 5 shows a voltammogram recorded in the basic solution at pH 5. During the direct scan, the current density response (curve 1, dotted line) exhibits a nucleation loop. The cathodic reaction begins at −750 mV. A shoulder is observed at potential smaller than −1200 mV corresponding to a diffusion controlled nickel deposition (limiting current density of 5.1 mA cm^{-2}). On the reverse scan, three peaks are observed as

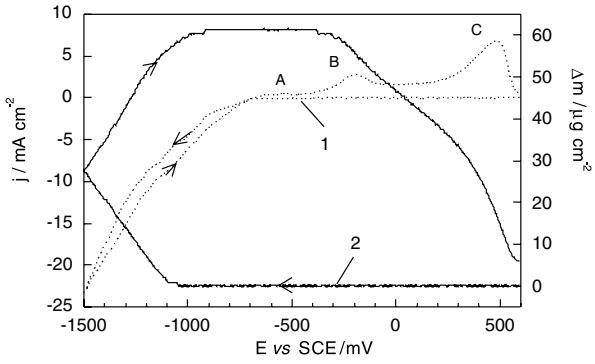

Fig. 5. Voltammogram recorded with the EQCM, basic solution pH 5, temperature 40 °C. Scan rate 10 mV s^{-1}. Curves: (1) current density response (dotted line) and (2) mass changes (solid line).

already observed in ammoniacal solutions [8]. As previously shown [17], peak A is poorly visible at this low temperature (40 °C); it may be related to the oxidation of hypophosphite [8, 9]. Other researchers have attributed this peak to the oxidation of adsorbed hydrogen [17, 18]. Peaks B and C are related to the two-step dissolution of the Ni–P alloy. Some authors attributed peak B to the dissolution of a crystalline phase and peak C to that of a P-rich Ni alloy phase [1, 19, 20]. However, such behaviour is often observed in the dissolution of pure nickel electrodeposits [21].

The charge used for the cathodic process, Q_c, was measured through integration of the current for the direct scan from −500 mV and reverse up to −500 mV, that is, just before the dissolution starts. It is equal to 1.4 C cm^{-2}, which, according to Faraday's law, would correspond to a deposited mass of 431 μg cm^{-2}, whereas the experimental one is only 61.5 μg cm^{-2}. This corresponds to a faradaic efficiency of 14%. The charge used for the dissolution process from −500 to +600 mV, Q_{dis}, is 0.27 C cm^{-2}. This anodic charge would correspond to a dissolved mass of 82.5 μg cm^{-2}. The dissolution efficiency, $\Delta m_{film}/\Delta m(Q_{dis.})$, is then smaller than unity, close to 75%. This behaviour indicates that, during the anodic process, parasitic electrochemical reactions, associated with a negligible mass loss, occur in parallel with the dissolution of the film. This might correspond to the oxidation of the hypophosphite species adsorbed on the electrode and/or of the occluded hydrogen.

The effect of the hypophosphite and nickel sulfate concentrations and of the pH has been investigated. Figure 6 shows the result for a nickel sulfate concentration of 0.15 M (electrolyte 3c). The deposition starts at a lower polarization than in the basic solution. The cathodic wave shows a shoulder, which indicates that nickel deposition exhibits a diffusion control behaviour. The limiting current density is about 7.7 mA cm^{-2}, which is about 1.5 times greater than in the basic solution (Figure 5), in agreement with the nickel sulfate relative concentrations. In the potential range between −800 and −1150 mV (first cathodic wave), the cathodic

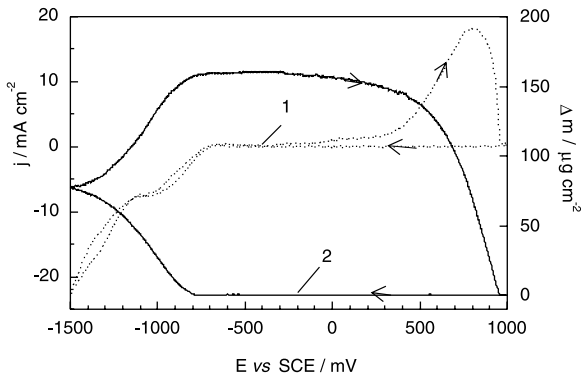

Fig. 6. Voltammogram recorded with the EQCM, solution with 0.15 M dm^{-3} $NiSO_4$, pH 5, temperature 40 °C. Scan rate 10 mV s^{-1}. Curves: (1) current density response (dotted line) and (2) mass changes (solid line).

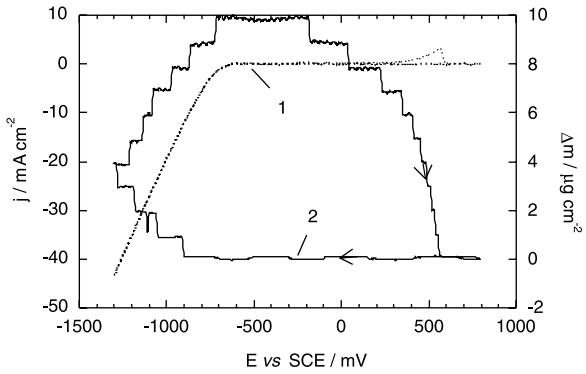

Fig. 7. Voltammogram recorded with the ECQM, basic solution pH 4, temperature 40 °C. Scan rate 10 mV s^{-1}. Curves: (1) current density response (dotted line) and (2) mass changes (solid line).

current efficiency is close to 85%, that is, much higher than for the basic solution. At potentials more negative, the efficiency decreases due to the proton reduction, which becomes predominant.

The intensity of peak B is markedly reduced and that of peak C is increased. The dissolution efficiency is 72%.

Figure 7 shows the voltammetric curve recorded in a solution of pH 4. The cathodic reaction is markedly depolarized, but mainly corresponds to the reduction of protons. The cathodic efficiency is drastically decreased to 1%. The dissolution efficiency is also decreased to 60%. A similar behaviour is observed for electrolytes with low hypophosphite (electrolyte 2a) or low nickel sulfate (electrolyte 3a) concentrations.

Table 3 summarizes the results of the voltammetric investigation with the EQCM. Not only the cathodic efficiency but also the dissolution efficiency are smaller than 1. In both cases, parasitic electrochemical reactions occur in parallel with the deposition or the dissolution processes corresponding to a negligible mass change. For the cathodic process, it is well known that reduction of the protons of the solvent occurs leading to hydrogen evolution and possibly its incorporation in the deposit.

Table 3. Cyclic voltammetric results

Electrolyte	Q_c* /C cm^{-2}	Q_{dis}† /C cm^{-2}	Q_{dis}/Q_c‡	$\Delta m_{film}/\Delta mQ_c$§	$\Delta m_{film}/\Delta m(Q_{dis})$§
1a	2.40	0.053	0.02	0.01	0.6 ± 0.05
1b (basic)	1.40	0.27	0.19	0.14	0.7 ± 0.05
1c	0.68	0.151	0.22	0.15	0.6 ± 0.05
2a	0.94	0.201	0.21	0.23	
2c	1.19	0.231	0.19	0.15	0.7 ± 0.05
3a	2.30	0.006	0.003	0.01	
3c	1.40	0.736	0.53	0.41	0.7 ± 0.05

* Q_c, charge used during the cathodic reduction (from −500 to −500 mV).

† Q_{dis} anodic charge used for the dissolution of the layers (from −500 to 1000 mV).

‡ Q_{dis}/Q_c ratio.

§ $\Delta m_{film}/\Delta m(Q_c)$ and $\Delta m_{film}/\Delta m(Q_{dis})$, ratio of the mass of the deposit by the mass calculated from Faraday's law, respectively, for the reduction and the dissolution processes.

During the anodic process it is more likely that at least part of the incorporated hydrogen might desorb and undergo an oxidation reaction [10, 11]; oxidation of the hypophosphite species may also account for a dissolution efficiency smaller than unity.

4. Discussion

Bonino et al. showed, through thermodesorption analysis, that hydrogen desorption evolution occcured during heating of electrodeposited amorphous Ni–P alloys [16]. At temperatures below 300 °C, hydrogen would be desorbed from the Ni–P solid solution. It is likely that, in our experiments, the mass decrease is related to the hydrogen desorption. The two-step decrease may be related to the desorption of hydrogen from the crystalline and the amorphous phases.

Comparison between the results of the thermodesorption and the voltammetry clearly shows that incorporated hydrogen has two origins: the cathodic and the anodic reactions. The amount of incorporated hydrogen decreases when the pH or when the nickel sulfate concentration increases. In both cases, the plating rate, as well as the current efficiency, increase. These features suggest that the incorporation of hydrogen is directly related to the reduction of protons from the solvent. More surprisingly, the incorporated hydrogen increases when the hypophosphite concentration is increased, though the plating rate is increased. This suggests that part of the incorporated hydrogen stems from the anodic processes. These observations can be explained by considering the following reaction path.

The electroless process results from anodic processes (Reactions 1 and 2) and reduction processes (Reactions 3 to 5) [22].

$$H_2PO_2^- \rightarrow HPO_2^- + H_{ads} \rightarrow H_{inc} \rightarrow 1/2H_2(\text{evolved}) \quad (1)$$

$$HPO_2^- + H_2O \rightarrow H_2PO_3^- + e^- + H^+ \quad (2)$$

$$Ni(II) + 2e^- \rightarrow Ni \quad (3)$$

$$H_2PO_2^- + 2H^+ + e^- \rightarrow P + 2\,H_2O \quad (4)$$

$$H^+ + e^- \rightarrow H_{ads} \rightarrow H_{inc} \rightarrow 1/2H_2(\text{evolved}) \quad (5)$$

Abrantes and coworkers showed that the oxidation was initiated by the adsorption of hyphophosphite on the catalytic surface, followed by the homolysis of its hydrogen bond [23–25]. This results in the formation of atomic and ionic radicals, as already shown [26] (Reaction 1). These radicals then promote nickel and hypophosphorus acid reduction to originate the NiP deposit. Reaction 1 produces adsorbed hydrogen, which can either evolve or incorporate into the deposit.

The cathodic Reaction 3 corresponds to the reduction of the nickel sulfate (written here, for simplicity, as a single step though it is often considered as a two-step process [27]). Reaction 4 expresses the incorporation of phosphorus. It can also be written as

$$Ni(II) + H_2PO_2^- + 2H^+ + e^- \rightarrow Ni{-}P + 2\,H_2O \quad (4')$$

Indeed, it is known that the reduction of hypophosphite does not occur separately but only in the presence of an inducing species such as nickel ions [28]. The reduction of these specie occur simultaneously with the reduction of protons (Reaction 5) which also leads to adsorbed hydrogen which can either incorporate into the growing deposit or evolve.

Both anodic and cathodic processes can lead to hydrogen evolution and/or incorporation. The low cathodic current efficiency is due to the importance of Reaction 5. The efficiency increases with increase in the nickel sulfate concentration (increase in Reaction 3) or the pH (decrease in Reaction 5). The phosphorus content in the films is about 14.5 wt % (i.e., 24 at %), which means that the rate of Reaction 4 is approximately four times smaller than that of Reaction 3. The plating rate depends on both anodic and cathodic processes. It increases when the concentration of hypophosphite increases, when the concentration of protons decreases or the concentration of nickel sulfate increases. The amount of incorporated hydrogen in the layers is the sum of the amount of hydrogen incorporated from the anodic reactions, $\Delta m\mathrm{H_a}$, and from the cathodic reactions, $\Delta m\mathrm{H_c}$, divided by the mass of the deposited film, Δm_{film}. $\Delta m\mathrm{H_a}$ is proportional to the concentration of hypophosphite through Reaction 1. $\Delta m\mathrm{H_c}$ is proportional to the concentration of protons through Reaction 5. The deposited mass, Δm_{film}, depends on Reactions 3 and 4. The amount of incorporated hydrogen will decrease when the pH or the nickel sulfate concentration increase. It will also increase when the concentration of hypophosphite increases. This reaction path allows good qualitative description of most of the experimental features.

Acknowledgements

The authors wish to thank Dr F. Faudot for the thermogravimetric measurements. This work was carried out as part of the '*Programme d'appui à la recherche scientifique*' of Morroco.

References

1. U. Hofmann and K.G. Weil, *Dechema-Monographien* **121** (1990) 257.
2. M. Benje, U. Hofmann, U. Pitterman and K.G. Weil, *Ber. Bunsenges. Phys. Chem.* **92** (1988) 1257.
3. W. Riedel, Galvanotechnik **81** (3) (1990) 842.
4. G.O. Mallory and V.A. Loyd, *Plat. Surf. Finish.* **72** (1985) 52.
5. T. Kobayashi, J. Ishibashi, S. Mononobe, M. Ohtsu and H. Honma, *J. Electrochem. Soc.* **147** (2000) 1046.

6. Chun-Jen Chen and Kwang-Lung Lin, *J. Electrochem. Soc.* **146** (1999) 137.
7. M. Cherkaoui, A. Srhiri and E. Chassaing, *Plat. Surf. Finish.* **79** (1992) 68.
8. M. Ebntouhami, M. Cherkaoui, A. Srhiri, A. Benbachir and E. Chassaing, *J. Appl. Electrochem.* **26** (1996) 487.
9. M. Ebntouhami, E. Chassaing and M.Cherkaoui, *Electrochim. Acta* **43** (1998) 1721.
10. J. Chitty, A. Pertuz, H. Hintermann, M.H. Staia and E.S. Puchi, *Thin Solid Films* **308–309** (1997) 430.
11. R.L. Zeller III and U. Landau, *J. Electrochem. Soc.* **137** (1990) 1107.
12. J.J. Kelly, K.M.A. Rahman, C.J. Durning and A.C. West, *J. Electrochem. Soc.* **145** (1998) 492.
13. M. Saaoudi, M. Ebntouhami, M. Cherkaoui, A. Srhiri, A. Ben Bachir, M. Elhark and A. Tanji, *French patent 2 754 831* (1998).
14. I. Bakonyi, A. Cziraki, I. Nagy and M. Hosso, *Z. Metallkunde* **77** (1986) 425.
15. K-H. Hur, *J. Mat Sci.* **25** (1990) 2573.
16. J-P. Bonino, S. Bruet-Hotellaz, C. Bories, P. Pouderoux and A. Rousset, *J. Appl. Electrochem.* **27** (1997) 1193.
17. C. Gabrielli and F. Raulin, *J. Appl. Electrochem.* **1** (1971) 167.
18. J. Crousier, Z. Hanane and J-P. Crousier, *Thin Solid Films* **248** (1994) 51.
19. R. Stevanovic, J. Stevanovic and A. Despic, *J. Appl. Electrochem.* **29** (1999) 747.
20. J. Crousier, Z. Hanane and J-P. Crousier, *Electrochim. Acta* **38** (1993) 261.
21. L.M. Abrantes, M.C. Oliveira, J.P. Bellier and J. Lecoeur, *Electrochim. Acta* **39** (1994) 1915.
22. I. Ohno, *Mater. Sci. Eng.* **A146** (1991) 33.
23. L.M. Abrantes and J.P. Correia, *J. Electrochem. Soc.* **141** (1994) 2356.
24. L.M. Abrantes, M.C. Oliveira and E. Vieil, *Electrochim. Acta* **41** (1996) 1515.
25. L.M. Abrantes and M.C. Oliveira, *J. Electrochem. Soc.* **147** (2000) 2981.
26. L.V. Sastri, R.E. Huie and P. Neta, *J. Phys. Chem.* **94** (1990) 1895.
27. E. Chassaing, M. Joussellin and R. Wiart, *J. Electroanal. Chem.* **157** (1983) 75.
28. A. Brenner, 'Electrodeposition of Alloys', Vol. 1–2 (Academic Press, New York, 1963).